



# HHS Public Access

Author manuscript

*Gastroenterology*. Author manuscript; available in PMC 2017 February 01.

Published in final edited form as:

*Gastroenterology*. 2016 February ; 150(2): 488–498. doi:10.1053/j.gastro.2015.10.008.

## Hepatic Arterial Infusion of Low-Density Lipoprotein Docosahexaenoic Acid Nanoparticles Selectively Disrupts Redox Balance in Hepatoma cells and Reduces Growth of Orthotopic Liver Tumors in Rats

Xiaodong Wen<sup>1</sup>, Lacy Reynolds<sup>1</sup>, Rohit S. Mulik<sup>1</sup>, Soo Young Kim<sup>1</sup>, Tim Van Treuren<sup>1</sup>, Liem H. Nguyen<sup>2,3</sup>, Hao Zhu<sup>2,3</sup>, and Ian R. Corbin<sup>1,3,\*</sup>

<sup>1</sup>Advanced Imaging Research Center, University of Texas Southwestern Medical Center at Dallas, Dallas, TX 75390, USA

<sup>2</sup>Children's Research Institute Department of Pediatrics, University of Texas Southwestern Medical Center at Dallas, Dallas, TX 75390, USA

<sup>3</sup>Internal Medicine Division of Liver and Digestive Diseases, University of Texas Southwestern Medical Center at Dallas, Dallas, TX 75390, USA

### Abstract

**Background & Aims**—Dietary intake of the natural omega-3 fatty acid docosahexaenoic acid (DHA) has been implicated in protecting patients with viral hepatitis B or C from developing hepatocellular carcinoma (HCC). Little is known about the effects of DHA on established solid tumors. Herein, we describe a low-density lipoprotein (LDL)-based nanoparticle that acts as a transporter for unesterified DHA (LDL–DHA) and demonstrates selective cytotoxicity towards

\*Correspondence should be addressed to: Dr. Ian R. Corbin, Advanced Imaging Research Center, 5323 Harry Hines Blvd., Dallas, Texas, 75390, Phone: 214-645-7044; Fax: 214-645-2744; ian.corbin@utsouthwestern.edu.

**Publisher's Disclaimer:** This is a PDF file of an unedited manuscript that has been accepted for publication. As a service to our customers we are providing this early version of the manuscript. The manuscript will undergo copyediting, typesetting, and review of the resulting proof before it is published in its final citable form. Please note that during the production process errors may be discovered which could affect the content, and all legal disclaimers that apply to the journal pertain.

### Conflict of Interest:

None

### Author's Contributions:

---

Xiaodong Wen	Acquisition and analysis of data; contribution to design; draft article
Lacy Reynolds	Acquisition and analysis of data; critical revision of content; draft article
Rohit S. Mulik	Acquisition and analysis of data; critical revision of content; draft article
Soo Young Kim	Acquisition and analysis of data
Tim Van Treuren	Acquisition and analysis of data
Liem H. Nguyen	Acquisition and analysis of data
Hao Zhu	Contribution to design and interpretation of data
Ian R. Corbin	Contribution to conception and design; Analysis and interpretation of data; Draft article and critical revision; Final approval for publication; Accountable for all aspects of work

---

HCC cells. We investigated the ability of LDL–DHA to reduce growth of orthotopic hepatomas in rats.

**Methods**—ACI rats were given intrahepatic injections of rat hepatoma cells (H4IIE); 24 tumor-bearing rats (mean tumor diameter, ~1 cm) were subject to a single hepatic artery injection of LDL nanoparticles (2 mg/kg) loaded with DHA (LDL–DHA), triolein (LDL–TO) or sham surgery controls. Tumor growth was measured by magnetic resonance imaging and other methods; tumor, liver and serum samples were collected and assessed by histochemical, immunofluorescence, biochemical and immunoblot analyses.

**Results**—Three days after administration of LDL–TO or sham surgery, the control rats had large, highly vascularized tumors that contained proliferating cells. However, rats given LDL–DHA had smaller, pale tumors that were devoid of vascular supply and greater than 80% of the tumor tissue was necrotic. Four to 6 days after injection of LDL–DHA, the tumors were 3-fold smaller than those of control rats. The liver tissue that surrounded the tumors showed no histologic or biochemical evidence of injury. Injection of LDL–DHA into the hepatic artery of rats selectively deregulated redox reactions in tumor tissues by: increasing levels of reactive oxygen species and lipid peroxidation, depleting and oxidizing glutathione and nicotinamide adenine dinucleotide phosphate, and significantly downregulating the antioxidant enzyme glutathione peroxidase-4. Remarkably, the redox balance in the surrounding liver was not disrupted.

**Conclusion**—LDL–DHA nanoparticle selectively kills hepatoma cells and reduces growth of orthotopic liver tumors in rats. It induces tumor-specific necrosis by selectively disrupting redox balance within the cancer cell.

## Keywords

Nanomedicine; liver cancer; n-3 fatty acids ROS; lipid peroxidation

## Introduction

Hepatocellular carcinoma (HCC) is the fifth most common cancer worldwide and is responsible for over a half a million deaths annually<sup>1</sup>. The incidence and mortality of HCC have steadily increased three-fold over the past two decades and it is now ranked as the fastest growing cause of cancer-related deaths in the United States<sup>2, 3</sup>. Moreover, estimates indicate that this increasing trend is expected to continue into the next decade<sup>4</sup>. Within the United States less than 20% of newly diagnosed HCC patients present at an early stage, which are amenable for curative therapies such as surgical resection, liver transplantation, or ablative techniques<sup>5</sup>. Of the remaining 80% of patients, 60% of HCC patients present with either intermediate or advanced stage disease. Unfortunately, the treatment options for these patients are limited, and even with the recently approved systemic multikinase inhibitor, Sorafenib, the 5-year survival rate for HCC remains <12%.<sup>3</sup> The poor prognosis of these patients highlights the need for more effective therapies. Natural products have and continue to be an invaluable source for anticancer drug discovery<sup>6</sup>. In recent years, the natural omega-3 fatty acid, docosahexaenoic acid (DHA) has been shown to possess promising anticancer properties<sup>7, 8</sup>. In fact, a study by Swanda *et al* recently reported that the dietary consumption of fish rich in omega-3 fatty acids protects against the development of HCC in

patients with hepatitis B or C infection<sup>9</sup>. Evidence for the beneficial effects of dietary DHA on established solid tumors, however, is sparse. Although numerous *in vitro* cell cultures studies have shown that unesterified omega-3 fatty acids have a potent dose-dependent cytotoxic effect on cancer cells<sup>10, 11</sup>, these doses of omega-3 fatty acid simply cannot be achieved *in vivo* at the local tumor site through dietary consumption of these lipids<sup>12</sup>. To address this issue, our lab has recently engineered a novel low-density lipoprotein (LDL) based nanoparticle that is uniformly reconstituted with unesterified DHA (herein referred to as LDL-DHA)<sup>13</sup>. We demonstrated that the LDL-DHA nanoparticle closely resembles native plasma LDL, and is an ideal transporter for DHA. Therapeutically, LDL-DHA nanoparticles proved to be selectively cytotoxic towards HCC cells. In a murine cell culture system, LDL-DHA is able to efficaciously kill HCC cells at doses that do not harm normal liver cells<sup>13</sup>. We later showed that the lethal anticancer actions of LDL-DHA nanoparticle treatment were mediated by the selective induction of lipid peroxidation and oxidative stress in the murine HCC cells. In the present study, we evaluate the *in vivo* anticancer efficacy of the LDL-DHA nanomedicine in an orthotopic syngeneic rat model of HCC.

## Materials and Methods

### Preparation of LDL-DHA

Human LDL was isolated from apheresis plasma of patients with familial hypercholesterolemia using sequential density gradient ultracentrifugation<sup>14</sup>. Incorporation of unesterified DHA (Nuchek Prep, INC) into LDL was performed by the reconstitution method as described in our previous publication<sup>13</sup>. Throughout these studies LDL reconstituted with triolein (LDL-TO) or oleic acid (LDL-OA) served as controls. Nanoparticle characterization (structure and composition) was performed as described previously<sup>13</sup> to ensure consistency of batch to batch preparations.

### Cell Culture and Animals

The rat hepatoma cell line, H4IIE, was maintained in Dulbecco's modified Eagle's medium (DMEM) containing 10% fetal bovine serum (FBS). Cells were grown at 37°C in an atmosphere of 5% CO<sub>2</sub> in a humidified incubator.

Adult ACI rats (175–195 g) were obtained from Harlan Laboratories, Inc. (Indianapolis, IN). Rats were housed under standard laboratory conditions with a 12 hour day/night cycle and were maintained on Purina rat chow and water *ad libitum* throughout the studies. All studies were approved by the University of Texas Southwestern Medical Center Animal Ethics Committee.

For details on the culture of mouse and human cells, hepatocyte isolation for primary hepatocyte culture, orthotopic HCC implantation, MRI detection of tumor size, hepatic artery injections, serum analyses, tissue pathology, cell viability and cell death assays please refer to the Experimental Procedure section in the Supporting Information.

### Measurements of Oxidative Stress

Determination of cell and tissue levels of lipid peroxidation, reactive oxygen species (ROS), protein-bound carbonyls, NADPH/NADP, GSH/GSSG and the redox potential of the glutathione redox couple are described in detail in the Experimental section in the Supporting Information.

### Western Blot and Immunohistochemistry

Detailed descriptions of western blot analysis performed on cell and tissue proteins and immunohistochemistry of tissue sections can be found in the Supporting Information.

### Statistical Evaluation

The results were expressed as mean  $\pm$  standard error. Analysis of variance (ANOVA) with Tukey's multiple comparison *post hoc* testing was used for evaluation of differences between groups. Differences with a P value less than 0.05 were deemed significant.

## Results

### Physicochemical Properties of LDL Nanoparticles

LDL-DHA nanoparticles were prepared by the reconstitution method described previously<sup>13</sup>. The physicochemical properties of the LDL-DHA were similar to those previously reported. The mono-dispersed nanoparticles had an average particle size of 20 nm, surface charge  $-25\text{mV}$  and DHA loading approximating 1152 molecules per LDL particle. More details of the LDL-DHA nanoparticle composition can be seen in Supplementary Fig. 1. The control LDL nanoparticles reconstituted with triolein (LDL-TO) or oleic acid (LDL-OA) were of similar size (23–24 nm) and zeta potential reading were  $-15\text{mV}$  and  $-25\text{mV}$  respectively. On average LDL-TO nanoparticles carried 344 triolein molecules, while LDL-OA carried 1700 molecules of oleic acid.

### LDL-DHA is able to Selectively Kill HCC Cells and Exhibits Significant Therapeutic Activity *In Vivo*

LDL-DHA dose response studies were performed in malignant H4IIE hepatoma cells and their syngeneic normal counterparts, ACI rat primary hepatocytes (Fig. 1A). The H4IIE cells were particularly sensitive to the LDL-DHA treatments, complete cell kill was achieved at  $60\ \mu\text{M}$  LDL-DHA. Meanwhile, the primary hepatocytes remained unharmed in this dose range. It was not until concentrations reached approximately  $125\text{--}130\ \mu\text{M}$  that primary hepatocytes started to experience cytotoxic effects of the treatment. To further demonstrate that the selective cytotoxic properties of LDL-DHA was not a rat specific effect, dose response studies were also performed in mouse and human hepatocyte and HCC cell lines (Supplementary Fig. 2). Similar to the rat cells, selective cytotoxicity was evident among the mouse (Hepa1C7, TIB-75) and human (SK-Hep1) HCC cells relative to their normal non-malignant counterparts. These findings are in keeping with our previous publication<sup>13</sup> and the work of others utilizing free polyunsaturated fatty acids (PUFAs)<sup>15, 16</sup>. Dose response curves of control LDL nanoparticles (LDL-OA (Supplementary Fig. 3) and LDL-TO (data not shown)) displayed no toxicity in either rat cell types over an extended dose range.

To visualize the ultrastructural changes occurring in the H4IIE cells following LDL–DHA treatment, transmission electron microscopy (TEM) was performed 24 hours after LDL nanoparticle exposure (Fig. 1B). Untreated control and the LDL–TO treated H4IIE cells displayed similarly healthy epithelial morphology. Conversely, toxicity from the LDL–DHA treatment could clearly be seen in many of the H4IIE cells. These cells adopted a more oval/spherical shape and nuclear chromatin condensation/fragmentation, along with disrupted plasma membrane. At higher magnification, dysmorphic mitochondria along with many autophagosomes/autolysosomes could be seen throughout their cytoplasm. Fluorescent markers of cell death (propidium iodide (PI) and Annexin-V) were also used to identify the pathways of cell death in the treated cells (Supplementary Fig. 4). The LDL–DHA treated H4IIE cells displayed strong fluorescence signal for both PI and Annexin-V, suggesting a mixed pattern of cell killing mediated by LDL–DHA. Neither untreated controls nor the LDL–TO treated cells displayed fluorescent signals for apoptosis or necrosis, indicating that these cells maintained good viability.

A local regional transarterial approach was taken to administer the LDL nanoparticles to the hepatoma bearing rats. This hepatic artery injection approach minimizes the systemic exposure of our nanoparticle drug in the animals and ensures that adequate concentrations of LDL nanoparticles reached the H4IIE tumors. Studies with fluorophore-labelled LDL nanoparticles (LDL–DiR) demonstrated that HAI was able to achieve high levels of LDL nanoparticle delivery to the hepatoma equaling or even surpassing that of the liver (Fig. 2A). Furthermore, fluorescent microscopy was able confirm *in situ* intracellular uptake of the LDL nanoparticle into liver and tumor cells (Fig 2B). Next, the therapeutic and biological effects of HAI of LDL–DHA were assessed three days following sham surgery or a single injection of LDL nanoparticles (Fig. 3).

Sham operated (n=5) and LDL–TO treated (n=7) animals similarly displayed large poorly differentiated HCC. These tumors were highly vascularized and histologic sections showed viable tissue that was actively proliferating. The LDL–DHA treated rats (n=12) had smaller pale tumors that were noticeably void of vascular supply. Histology later confirmed that LDL–DHA treated tumors had undergone complete necrosis (Fig. 3 and Supplementary Table 1). Surrounding the necrotic tumors were sharp boundaries of granulation-type tissues characterized by fibrous deposition and phagocytic cell infiltrates. Tissue sections depicted in Fig. 2 show a clear and definitive demarcation of necrotic tumor tissue and viable liver tissue. In addition, complementary immunohistochemical analyses for Ki-67 and cleaved caspase-3 staining were also performed on these tissue sections (Supplementary Fig. 5). Sham and LDL–TO treated tumors displayed abundant staining for proliferative activity (Ki-67). Sparse staining of cleaved-caspase-3 (apoptosis) was seen in the Sham and LDL–TO treated tumors. In contrast, staining for both Ki-67 and cleaved caspase-3 were noticeably absent in LDL–DHA treated tumors. Interestingly, the absence of cleaved caspase-3 staining suggests that *in vivo* tumors underwent a caspase independent cell death following LDL–DHA treatment.

Although the LDL–DHA treatment was able to severely induce pronounced damage to HCC tumors *in situ*, this nanomedicine proved to be highly selective, as the surrounding liver showed little to no evidence of injury. Accompanying serum biochemistry tests were

performed, they showed that the LDL–DHA treated animals actually had lower levels of the markers of liver injury, alanine aminotransferase (ALT) and aspartate aminotransferase (AST) compared to Sham and LDL–TO controls (Supplementary Table 2). All the other analytes in the serum biochemistry panel were unremarkable between the groups with the exception of albumin which was slightly lower for the LDL–DHA treated animals.

A subset of treated rats was also followed by non-invasive magnetic resonance imaging (MRI) to assess the treatment effect of LDL–DHA (Fig. 4). Tumor volume measurements followed 4–6 days after treatment revealed that LDL–DHA significantly inhibited the growth of the rat hepatoma approximately 3 fold compared to LDL–TO treated animals. These results were later validated in an additional cohort of rats evaluated 7 days following Sham and LDL nanoparticle treatments (Supplementary Fig. 6). Upon sacrifice LDL–DHA treated tumors were smaller (~2.5 fold) and pale in color compared to Sham and LDL–TO injected animals. Histology later confirmed that LDL–DHA was selectively cytotoxic to the HCC tumors without injuring the surrounding liver. In addition, serum biochemistry tests also consistently showed lower levels of ALT and AST in the LDL–DHA treated animals (Supplementary Table 3). At this time albumin levels were normalized in the LDL–DHA group; however, the blood urea nitrogen levels were slightly lower than controls.

Supplementary experiments were also performed in mice with *MYC*-induced liver tumors to demonstrate the anticancer effects of the LDL–DHA nanoparticles in an additional model of liver cancer. After only three systemic injections of LDL–DHA (4 mg/kg) the aggressive liver tumors in the *MYC* overexpressing mice already showed evidence of LDL–DHA anticancer cytotoxicity. These tumors had higher levels of damaging lipid peroxides (TBARS) and lower indices of cell proliferation compared to LDL–TO treated mice (Supplementary Fig. 7A,B). In addition, the LDL–DHA treated mice also had smaller abdominal girth indicative of suppressed tumor growth/hepatomegaly (Supplementary Fig. 7C).

### **LDL–DHA Killing of Cancer Cells is Mediated by Free Radical Rather than Oxygenase Enzymatic Activity**

DHA, like other PUFAs, can be the substrate for a number of oxygenase enzyme systems which include cyclooxygenase (COX), lipoxygenase (LOX) and cytochrome P450 (CYP450). To investigate the importance of these enzymatic pathways in the tumor cytotoxicity of LDL–DHA, specific inhibitors to each of these enzymes were evaluated in viability assays with LDL–DHA treated H4IIE cells. Supplementary Fig. 8A shows that known effective doses of 1-aminobenzotriazole (CYP450 inhibitor), NS-398 (a selective inhibitor of cyclooxygenase-2 (COX-2)), Nordihydroguaiaretic acid ((NDGA) a non-selective LOX inhibitor), and indomethacin (a nonselective inhibitor of COX1 and 2) were unable prevent the cytotoxicity induced by LDL–DHA. Given that none of these inhibitors were able to protect against LDL–DHA treatment, we next sought to examine the role of free radical mediated lipid peroxidation in this process. Vitamin E, a known free radical scavenger and inhibitor of lipid peroxidation, was able to effectively rescue the H4IIE cells from LDL–DHA cytotoxicity over a wide range of vitamin E concentrations (from 10  $\mu$ M–



200  $\mu\text{M}$ ) (Supplementary Fig. 8B). Overall, these findings suggest that the LDL–DHA tumor cytotoxicity is mediated by free radical propagated redox-stress.

### LDL–DHA Treatment Selectively Induces Redox-Stress in Cancer Cells

The cellular response to LDL–DHA treatment is characterized by a selective increase of redox stress within HCC cells. When H4IIE cells are exposed to LDL–DHA (40  $\mu\text{M}$ ) over a 48 hour period, significant increases in ROS and lipid peroxidation were detected by dihydroethidium (DHE) fluorescence and thiobarbituric acid reactive species (TBARS) measurements respectively (Fig. 5A and B). Under the same conditions of LDL–DHA treatment, primary ACI rat hepatocytes do not experience any increase in ROS or lipid peroxidation (Supplementary Fig. 9A and B). Finally, carbonyl levels were also assayed in the H4IIE cells before and after LDL nanoparticle treatment as a measure of protein oxidation. Once again, H4IIE cells demonstrated significant redox stress (6-fold increase in protein carbonylation), after LDL–DHA treatment compared to untreated and LDL-TO treated controls (Fig. 5C).

Parallel experiments examining *in situ* redox status were performed in tumor bearing rats after sham and LDL nanoparticle treatments. Strong DHE tissue staining was selectively detected in the HCC of LDL–DHA treated rats (Fig. 5D). Meanwhile, the DHE staining in the corresponding livers from the LDL–DHA injected animals remained unchanged from sham levels. Semi quantitative analysis indicated that the paired tumor/liver DHE fluorescence intensity ratio was on average 4 fold for LDL–DHA treated animals, while the ratios in Sham and LDL-TO treated animals was 1 and 0.7 respectively (Supplementary Fig. 10). Tissue lipid peroxidation, as measured by the TBARS indices, followed a similar trend as the DHE readings (Fig. 5E). While Sham and LDL-TO treated animals had similar TBARS tumor/liver ratios (approximately 1.7-fold), LDL–DHA administered animals had significantly higher tumor/liver ratio reaching on average 3.3 fold. Lastly, the level of tissue protein carbonyls was investigated using the 2,4-dinitrophenylhydrazine (DNPH) spectrometric method; however, no difference in the tumor/liver protein carbonyl ratios was detected across the groups of rats (Supplementary Fig. 11). The high amounts of interfering chromophores present in tissue that absorbs at 370 nm (e.g., haemoglobin, myoglobin, retinoids) likely precluded the accurate measurements of the protein adducts in these samples.<sup>17</sup>

### LDL–DHA Reduces the Antioxidant Enzymatic Capacity in HCC

Next, we sought to examine the status of the antioxidant enzymes superoxidase dismutase 1 (SOD-1), catalase and glutathione peroxidase 4 (GPx-4), following LDL nanoparticle treatments. In the H4IIE cell culture studies, LDL–DHA treatment significantly reduced GPx-4 protein expression relative to control LDL-TO treated cells (Fig. 6A and B). The expression levels of SOD-1 and catalase did not differ between these treatment groups. For the *in vivo* studies, the protein expression levels of the antioxidant enzymes three days after sham and LDL nanoparticle treatments are presented in Fig. 6C. In general, tumors tended to express less of the antioxidant enzymes compared to their corresponding liver. Densitometry analysis of the Western blots revealed that only tumor GPx-4 protein levels were significantly down-regulated after LDL–DHA treatment (Fig. 6D). These findings are

consistent with the *in vitro* results. Further analyses of the antioxidant enzymes were carried out in the subset of rats studied seven days post treatment (Supplementary Fig. 12). Tumor/liver ratios of GPx-4 and SOD-1 were significantly lower in LDL-DHA groups compared to the Sham and LDL-TO controls. The catalase tumor/liver ratio was similar between Sham and LDL-DHA treatment groups, but was significantly higher in the LDL-TO treated animals.

### Tumor Cells Selectively Experience Severe Deregulation of Redox Couples Following LDL-DHA Treatment

The metabolic redox couples NADPH/NADP and GSH/GSSG play a central role to the overall redox status of the cell. Cultures of H4IIE cells experienced significant reductions in both NADPH/NADP and GSH/GSSG after incubation with LDL-DHA (Fig. 7A). In both cases LDL-DHA caused the ratios of the redox couples to drop to 40%–50% of their LDL-TO treated or untreated controls.

Changes in the redox status following LDL-DHA administration were even more pronounced in the *in vivo* animal model (Fig. 7B). The ratios of NADPH/NADP and GSH/GSSG decreased precipitously in the tumors after the LDL-DHA treatment. The values for NADPH/NADP and GSH/GSSG ratios were approximately 25% and 18%, respectively, of that of the untreated and LDL-TO treated tumor controls. Despite the drastic changes in the tumor redox status following LDL-DHA treatment, redox homeostasis in the liver was maintained regardless of the treatment group.

In contrast to the simple ratios of GSH/GSSG, the glutathione half-cell potential ( $E_{\text{GSSG}/2\text{GSH}}$ ) utilizes the Nernst equation to quantitatively determine the reduction potential and reducing capacity of the sample and more accurately reflects the physiological state of the cell/tissue. Changes in the  $E_{\text{GSSG}/2\text{GSH}}$  have been shown to correlate with the biological status of the cell: where in general proliferating cells are reported to be  $\approx -240$  mV; differentiating cell  $\approx -200$  mV; quiescent cells are in between proliferation and differentiation states; and finally cell death occurs at potentials  $\approx -170$  mV and more positive.<sup>18</sup> The  $E_{\text{GSSG}/2\text{GSH}}$  for untreated, LDL-TO and LDL-DHA treated H4IIE cells were  $-232 \pm 4.1$  mV,  $-224 \pm 3.1$  mV, and  $-205 \pm 0.01$  mV respectively (Fig. 7A). The effects of LDL-DHA treatment on the tissue values for  $E_{\text{GSSG}/2\text{GSH}}$  were more striking (Fig. 7B). The liver  $E_{\text{GSSG}/2\text{GSH}}$  findings were similar to that for GSH/GSSG results, regardless of the treatment groups, a reduction potential value around  $-275$  mV was measured for all of the livers. The tumors from sham and LDL-TO treated animals had similar reduction potentials,  $-265.9 \pm 1.1$  mV and  $-251.4 \pm 6.5$  mV respectively. Lastly, the LDL-DHA treated tumor experienced a greater oxidative state as their reduction potential values shifted to  $-208.2 \pm 9.8$  mV.

## Discussion

The findings of the present study demonstrate how reformulation of DHA into a LDL nanoparticle expands the utility of this n-3 PUFA enabling its use as an anticancer therapeutic. The transarterial administration of LDL nanoparticles delivers DHA to tumors at sufficiently high concentrations to induce significant tumoricidal effects. Equally



compelling is the fact that the surrounding liver (which receives a similar dose of LDL-DHA) shows no evidence of injury or hepatotoxicity. While most chemoembolic treatments delivered via the transarterial route target HCC, accompanying injury to the surrounding liver is common<sup>19</sup> and in some rare clinical cases lobar atrophy or even fatal liver failure can occur<sup>20</sup>. Locoregional LDL-DHA treatment was highly selective for HCC, discrete boundaries of tumor necrosis and reactive fibrosis could be seen next to healthy hepatocytes. In fact, the serum markers of hepatocellular injury, ALT and AST, were significantly lower in the LDL-DHA treated animals than the Sham or LDL-TO treated rats. This suggests that LDL-DHA treatments are potentially beneficial to the surrounding normal liver by reducing hepatocellular injury. This is in keeping with anti-inflammatory and pro-resolving properties of DHA.

One of the hallmark features of the LDL-DHA treatment is the selective induction of redox stress in the H4IIE cells and tumors, while under equivalent conditions, normal cells and tissues remain unharmed. It is now well accepted in oncology that cancer cells augment and promote higher levels of oxidative stress<sup>21, 22</sup>. This pro-oxidant state is thought to maintain and drive the progression of the malignant phenotype<sup>23, 24</sup>. The findings from the present study support this observation as the poorly differentiated fast growing H4IIE tumors are associated with higher levels of lipid peroxidation, overall lower amounts of antioxidant enzymes, and trends towards lower ratios of GSH/GSSG and NADH/NADP than the surrounding normal liver. Elevated levels of oxidative stress, however, also predisposes neoplastic cells to injury from further ROS insults induced by exogenous agents. Under the same conditions normal cells effectively buffer the ROS challenge as their basal levels of oxidative stress are low and their antioxidative capacity is fully intact. We propose that the LDL-DHA nanotherapy operates under similar principles.

Once the LDL nanoparticle is endocytosed and degraded in the cell, the released DHA encounters drastically different environments in normal versus malignant cells. Within the normal cell, oxidative stress levels are low and as such DHA is not readily attacked by ROS. Instead, the cell actively converts the pool of non-esterified DHA to an acyl CoA derivative to maintain low concentrations of non-esterified fatty acids<sup>25</sup>. As a fatty acylCoA, DHA is rapidly esterified into neutral and polar lipids, while minor fractions undergo microsomal oxidation. Conversely, within the cancer cell, high concentrations of ROS likely readily attack the bisallylic hydrogens in the DHA molecule allowing lipid peroxidation to rapidly propagate throughout the cell. The magnitude of the lipid peroxidation process becomes significantly amplified when one considers that a single LDL-DHA nanoparticle transports over 1100 DHA molecules, a single LDL receptor transports scores of LDL per day (LDL receptor recycle time~20mins) and that a liver cell typically expresses between 15,000 and 70,000 LDL receptors<sup>26</sup>.

The pathological sequelae that arise from this massive lipid peroxidation undoubtedly involves damaged cell membranes, but equally destructive is the copious generation of reactive aldehyde end-products<sup>27</sup>. The  $\alpha,\beta$ -unsaturated aldehydes, such as malondialdehyde (MDA), are particularly pervasive as they diffuse within or across cells to attack distant targets from their site of origin<sup>28</sup>. These aldehydes react with most biomolecules to form adducts<sup>28</sup>. Evidence of this activity is seen by the markedly increased amount of protein

adducts (protein-carbonyls) in the LDL–DHA treated H4IIE cells. Once formed the adducts irreversibly alter the protein structure, ultimately leading to protein dysfunction. The collective deleterious effects of lipid peroxidation on cellular organelles is evident in the TEM of the LDL–DHA treated H4IIE cells. Our results are consistent with others<sup>29</sup> in showing that apoptotic and necrotic cell death can arise from extensive lipid peroxidation and aldehyde generation.

In addition to the cellular damage described above, the oxidized products of DHA also significantly cripple the antioxidative capacity of HCC cells/tumors. To prevent the accumulation of toxic  $\alpha,\beta$ -unsaturated lipid aldehydes within the cell, phase II detoxification reactions conjugate intracellular glutathione with the aldehydes (via glutathione S-transferase (GST)) to facilitate their active export from the cell<sup>30</sup>. The high concentrations and activity of GSH and GST within the cell enables this pathway to function as a high capacity detoxification system<sup>31</sup>. This in fact turns out to be the major route of aldehyde detoxification and elimination within the cell<sup>32</sup>. The efficiency of this system, however, ultimately serves to the detriment of the cancer cell as intracellular GSH pools are rapidly depleted following LDL–DHA treatment. Several other groups have also reported that GSH levels become significantly reduced in cancer cells after DHA exposure<sup>33, 34</sup>. As a result of the GSH depletion, the cells capacities to buffer oxidative challenges are greatly diminished. The significant reductions in the HCC's GSH/GSSG ratio and the GSH reduction potential (reducing capacity) clearly reveal the severe redox dysregulation induced by the LDL–DHA treatment. Under these strained conditions the NADPH/NADP couple is unable to provide sufficient reducing equivalents to the GSH system as the equilibrium of this couple is also shifted to a more oxidized state.

The ROS stress incited by LDL–DHA treatment is further exacerbated by the inhibitory effects of DHA on SOD-1 and GPx-4. This is particularly pertinent in the current setting, since GPx-4 is the only glutathione peroxidase known to directly act on phospholipid hydroperoxides, and thus is critical in protecting against lipid peroxidation<sup>35</sup>. Studies by Tuller *et al* and Ding *et al* have shown that DHA down-regulates the expression of SOD-1 and GPx-4 in cancer cells<sup>36, 37</sup>. Overall, we see that LDL–DHA treatment not only increases oxidation potential by initiating lipid peroxidation, reactive aldehyde generation and GSH depletion within malignant cells, but it also suppresses their antioxidant enzyme system, which further enhances the levels of oxidative stress ultimately ushering the demise of the cancer cell.

In conclusion, our study demonstrates that LDL–DHA nanoparticles have potent anti-cancer activity. Unlike other transarterial therapies the LDL–DHA nanoparticle is fully biocompatible, non-embolic and highly selective for its tumor target making it an attractive therapeutic alternative for other locoregional cancer indications. Future experiments will include long term survival studies to evaluate the therapeutic benefits provided by repeated LDL–DHA treatments.

## Supplementary Material

Refer to Web version on PubMed Central for supplementary material.

## ACKNOWLEDGMENT

We thank Dr. Mary Wight-Carter for providing histopathology expertise and Mr. John Shelton for his technical experimental assistance. We would also like to thank Mrs. Denise Ramirez from the UTSW Whole Brain Microscopy Facility (WBMF) in the Department of Neurology and Neurotherapeutics for assistance with slide scanning.

### Financial Support:

This work was supported in part by the American Gastroenterological Association (AGA) Research Foundation Scholar Award (IC), the Southwestern Small Animal Imaging Research Program (SW-SAIRP) (NCI U24 CA126608), the Cancer Center Support Grant (5P30 CA 142543-05) and the University of Texas Southwestern Medical Center President's Research Council Award (IC).

## Abbreviations

<b>HCC</b>	hepatocellular carcinoma
<b>DHA</b>	Docosahexaenoic acid
<b>LDL</b>	Low-density lipoprotein
<b>LDL-DHA</b>	Low-density lipoprotein uniformly loaded with docosahexaenoic acid
<b>LDL-DiR</b>	Low-density lipoprotein labelled with the lipophilic carbocyanine dye DiR (1,1'-Dioctadecyl-3,3,3',3'-Tetramethylindotricarbocyanine Iodide)
<b>LDL-TO</b>	Low-density lipoprotein uniformly loaded with triolein
<b>LDL-OA</b>	Low-density lipoprotein uniformly loaded with oleic acid
<b>DMEM</b>	Dulbecco's Modified Eagle's Medium
<b>FBS</b>	Fetal bovine serum
<b>ROS</b>	Reactive oxygen species
<b>NADP</b>	Oxidized Nicotinamide adenine dinucleotide phosphate
<b>NADPH</b>	Reduced Nicotinamide adenine dinucleotide phosphate
<b>GSH</b>	Reduced Glutathione
<b>GSSG</b>	Oxidized Glutathione
<b>ANOVA</b>	Analysis of variance
<b>PUFA</b>	Polyunsaturated fatty acid
<b>TEM</b>	Transmission electron microscopy
<b>PI</b>	Propidium iodide
<b>MRI</b>	Magnetic resonance imaging
<b>ALT</b>	Alanine aminotransferase
<b>AST</b>	Aspartate aminotransferase
<b>COX</b>	cyclooxygenase
<b>LOX</b>	Lipoxygenase

<b>CYP450</b>	Cytochrome P450
<b>NDGA</b>	Nordihydroguaiaretic acid
<b>DHE</b>	Dihydroethidium
<b>TBARS</b>	thiobarbituric acid reactive species
<b>DNPH</b>	2,4-Dinitrophenylhydrazine
<b>SOD-1</b>	Superoxidase dismutase 1
<b>GPx-4</b>	Glutathione peroxidase 4
<b>MDA</b>	Malondialdehyde
<b>GST</b>	Glutathione S-transferase

## References

1. Gomaa AI, Khan SA, Toledano MB, et al. Hepatocellular carcinoma: epidemiology, risk factors and pathogenesis. *World J Gastroenterol.* 2008; 14:4300–4308. [PubMed: 18666317]
2. El-Serag HB. Epidemiology of hepatocellular carcinoma in USA. *Hepato Res.* 2007; 37(Suppl 2):S88–S94. [PubMed: 17877502]
3. El-Serag HB. Hepatocellular carcinoma. *N Engl J Med.* 2011; 365:1118–1127. [PubMed: 21992124]
4. El-Serag HB. Epidemiology of viral hepatitis and hepatocellular carcinoma. *Gastroenterology.* 2012; 142:1264–1273. e1. [PubMed: 22537432]
5. El-Serag HB, Siegel AB, Davila JA, et al. Treatment and outcomes of treating of hepatocellular carcinoma among Medicare recipients in the United States: A population-based study. *Journal of Hepatology.* 2006; 44:158–166. [PubMed: 16290309]
6. Newman DJ, Cragg GM. Natural products as sources of new drugs over the last 25 years. *J Nat Prod.* 2007; 70:461–477. [PubMed: 17309302]
7. Siddiqui RA, Harvey K, Stillwell W. Anticancer properties of oxidation products of docosahexaenoic acid. *Chem Phys Lipids.* 2008; 153:47–56. [PubMed: 18343223]
8. Berquin IM, Edwards IJ, Chen YQ. Multi-targeted therapy of cancer by omega-3 fatty acids. *Cancer Letters.* 2008; 269:363–377. [PubMed: 18479809]
9. Sawada N, Inoue M, Iwasaki M, et al. Consumption of n-3 Fatty Acids and Fish Reduces Risk of Hepatocellular Carcinoma. *Gastroenterology.* 2012; 142:1468–1475. [PubMed: 22342990]
10. O’Flaherty JT, Hu Y, Wooten RE, et al. 15-Lipoxygenase Metabolites of Docosahexaenoic Acid Inhibit Prostate Cancer Cell Proliferation and Survival. *PLoS ONE.* 2012; 7:e45480. [PubMed: 23029040]
11. Kang KS, Wang P, Yamabe N, et al. Docosahexaenoic acid induces apoptosis in MCF-7 cells in vitro and in vivo via reactive oxygen species formation and caspase 8 activation. *PLoS One.* 2010; 5:e10296. [PubMed: 20421971]
12. Conquer JA, Holub BJ. Effect of supplementation with different doses of DHA on the levels of circulating DHA as non-esterified fatty acid in subjects of Asian Indian background. *J Lipid Res.* 1998; 39:286–292. [PubMed: 9507989]
13. Reynolds L, Mulik RS, Wen X, et al. Low-density lipoprotein-mediated delivery of docosahexaenoic acid selectively kills murine liver cancer cells. *Nanomedicine.* 2014:1–19.
14. Lund-Katz S, Laplaud PM, Phillips MC, et al. Apolipoprotein B-100 conformation and particle surface charge in human LDL subspecies: implication for LDL receptor interaction. *Biochemistry.* 1998; 37:12867–12874. [PubMed: 9737865]

15. Das UN, Huang YS, Begin ME, et al. Uptake and distribution of cis-unsaturated fatty acids and their effect on free radical generation in normal and tumor cells in vitro. *Free Radic Biol Med.* 1987; 3:9–14. [PubMed: 3040539]
16. Grammatikos SI, Subbaiah PV, Victor TA, et al. n-3 and n-6 fatty acid processing and growth effects in neoplastic and non-cancerous human mammary epithelial cell lines. *Br J Cancer.* 1994; 70:219–227. [PubMed: 8054269]
17. Dalle-Donne I, Rossi R, Giustarini D, et al. Protein carbonyl groups as biomarkers of oxidative stress. *Clin Chim Acta.* 2003; 329:23–38. [PubMed: 12589963]
18. Schafer FQ, Buettner GR. Redox environment of the cell as viewed through the redox state of the glutathione disulfide/glutathione couple. *Free Radic Biol Med.* 2001; 30:1191–1212. [PubMed: 11368918]
19. Li X, Zheng CS, Feng GS, et al. An implantable rat liver tumor model for experimental transarterial chemoembolization therapy and its imaging features. *World J Gastroenterol.* 2002; 8:1035–1039. [PubMed: 12439920]
20. Clark TW. Complications of hepatic chemoembolization. *Semin Intervent Radiol.* 2006; 23:119–125. [PubMed: 21326755]
21. Toyokuni S, Okamoto K, Yodoi J, et al. Persistent oxidative stress in cancer. *FEBS Letters.* 1995; 358:1–3. [PubMed: 7821417]
22. Szatrowski TP, Nathan CF. Production of large amounts of hydrogen peroxide by human tumor cells. *Cancer Res.* 1991; 51:794–798. [PubMed: 1846317]
23. Burdon RH. Superoxide and hydrogen peroxide in relation to mammalian cell proliferation. *Free Radic Biol Med.* 1995; 18:775–794. [PubMed: 7750801]
24. Behrend L, Henderson G, Zwacka RM. Reactive oxygen species in oncogenic transformation. *Biochem Soc Trans.* 2003; 31:1441–1444. [PubMed: 14641084]
25. Jump DB, Botolin D, Wang Y, et al. Docosahexaenoic acid (DHA) and hepatic gene transcription. *Chem Phys Lipids.* 2008; 153:3–13. [PubMed: 18343222]
26. Ratushny, AV.; Ignatieva, EV.; Matushkin, Y., et al. Mathematical Model of Cholesterol Biosynthesis Regulation in the Cell. Proceedings of the Second International Conference on Bioinformatics of Genome Regulation and Structure; Novosibirsk, Russia. 2000;
27. Kawai Y, Takeda S, Terao J. Lipidomic analysis for lipid peroxidation-derived aldehydes using gas chromatography-mass spectrometry. *Chem Res Toxicol.* 2007; 20:99–107. [PubMed: 17226932]
28. Gueraud F, Atalay M, Bresgen N, et al. Chemistry and biochemistry of lipid peroxidation products. *Free Radic Res.* 2010; 44:1098–1124. [PubMed: 20836659]
29. Ayala A, Mu #xf1, et al. Lipid Peroxidation: Production, Metabolism, and Signaling Mechanisms of Malondialdehyde and 4-Hydroxy-2-Nonenal. *Oxidative Medicine and Cellular Longevity.* 2014; 2014:31.
30. Long EK, Picklo MJ Sr. Trans-4-hydroxy-2-hexenal, a product of n-3 fatty acid peroxidation: make some room HNE. *Free Radic Biol Med.* 2010; 49:1–8. [PubMed: 20353821]
31. Hayes JD, McLellan LI. Glutathione and glutathione-dependent enzymes represent a co-ordinately regulated defence against oxidative stress. *Free Radic Res.* 1999; 31:273–300. [PubMed: 10517533]
32. Hartley DP, Ruth JA, Petersen DR. The hepatocellular metabolism of 4-hydroxynonenal by alcohol dehydrogenase, aldehyde dehydrogenase, and glutathione S-transferase. *Arch Biochem Biophys.* 1995; 316:197–205. [PubMed: 7840616]
33. Leonardi F, Attorri L, Benedetto RD, et al. Effect of arachidonic, eicosapentaenoic and docosahexaenoic acids on the oxidative status of C6 glioma cells. *Free Radical Research.* 2005; 39:865–874. [PubMed: 16036367]
34. Merendino N, Loppi B, D'Aquino M, et al. Docosahexaenoic acid induces apoptosis in the human PaCa-44 pancreatic cancer cell line by active reduced glutathione extrusion and lipid peroxidation. *Nutr Cancer.* 2005; 52:225–233. [PubMed: 16201853]
35. Imai H, Nakagawa Y. Biological significance of phospholipid hydroperoxide glutathione peroxidase (PHGPx, GPx4) in mammalian cells. *Free Radic Biol Med.* 2003; 34:145–169. [PubMed: 12521597]

36. Tuller ER, Beavers CT, Lou JR, et al. Docosahexaenoic acid inhibits superoxide dismutase 1 gene transcription in human cancer cells: the involvement of peroxisome proliferator-activated receptor alpha and hypoxia-inducible factor-2alpha signaling. *Mol Pharmacol.* 2009; 76:588–595. [PubMed: 19528198]
37. Ding WQ, Lind SE. Phospholipid hydroperoxide glutathione peroxidase plays a role in protecting cancer cells from docosahexaenoic acid-induced cytotoxicity. *Mol Cancer Ther.* 2007; 6:1467–1474. [PubMed: 17431126]



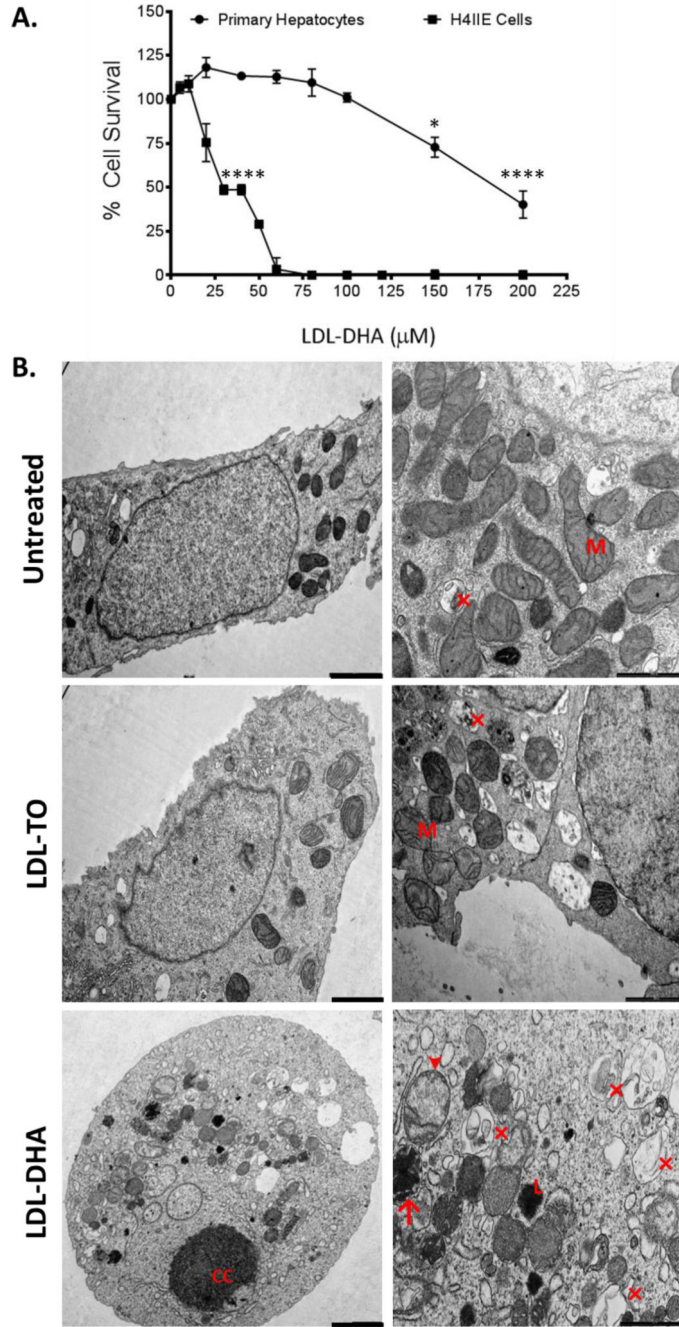


**Figure 1. Effects of LDL nanoparticles on primary hepatocytes and H4IIE cells**  
**(A)** MTS dose response assay of ACI rat primary hepatocytes and H4IIE cells to LDL–DHA (0–200 μM). Experiments were performed in triplicate wells with at least three independent runs. Results are expressed as mean ± SEM. \*, P 0.05; \*\*\*\*, P 0.0001 versus corresponding untreated group. All readings after 25 μM are significant at P 0.0001 for the H4IIE cells. **(B)** Transmission electron microscopy of H4IIE cells at baseline (untreated) and those treated with LDL–TO and LDL–DHA for 24 hours. Left panel (2000 nm magnification bar) right panel (1000 nm magnification bar). CC, nuclear chromatin condensation; M,

mitochondria; Arrow head denotes swollen dysmorphic mitochondria; arrow condensed mitochondria; (x) autophagosome/autolysosome; L, lysosome.

Author Manuscript

Author Manuscript

Author Manuscript

Author Manuscript

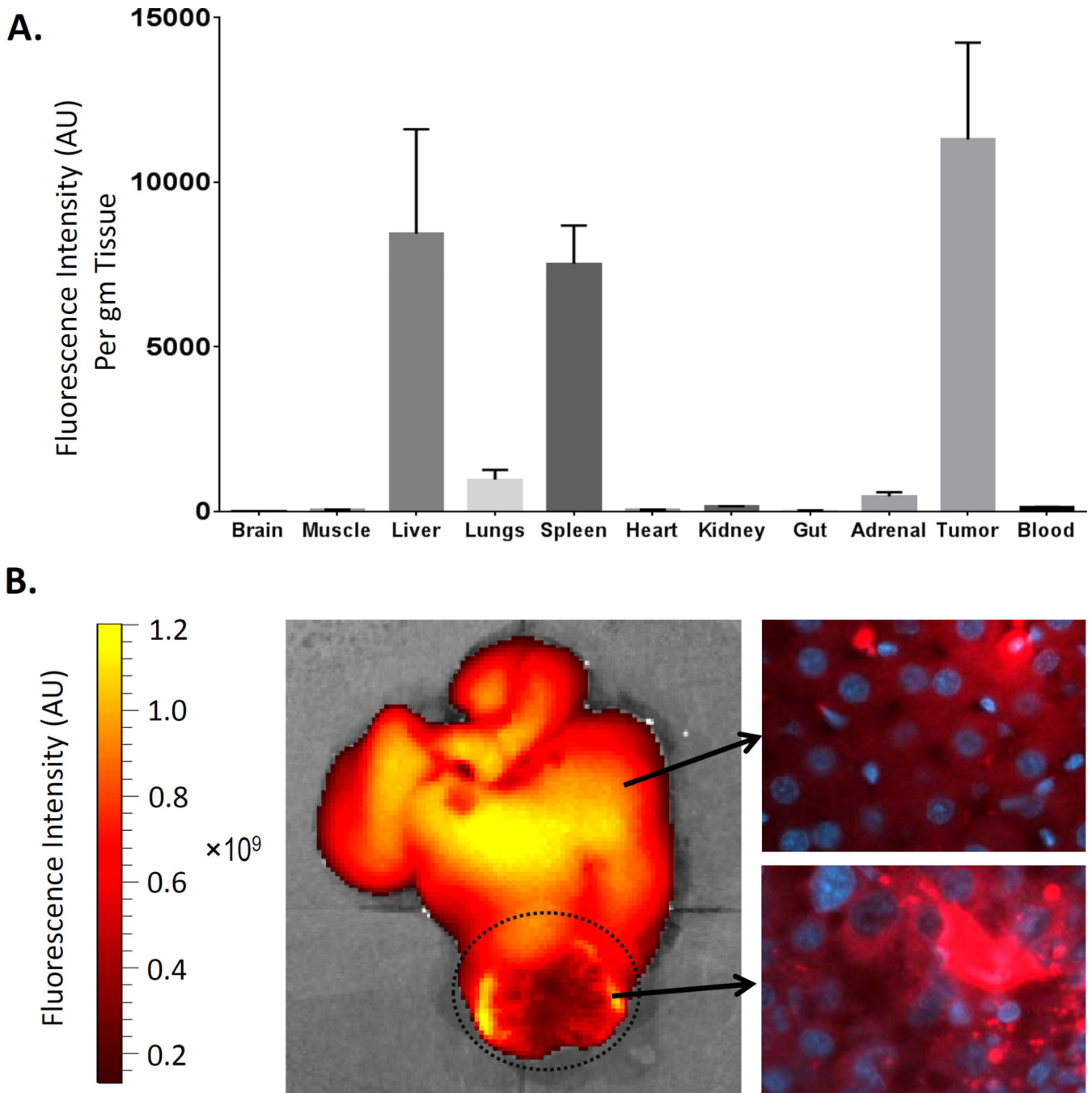


**Figure 2. Biodistribution and fluorescent imaging of LDL-DiR four hours following hepatic artery injection in HCC bearing rats**

(A) Data units are DiR fluorescence intensity per gram of tissue. Blood readings are measured in DiR fluorescence intensity per mL of blood. Data are expressed as mean  $\pm$  SEM. (B) Representative fluorescence image of excised liver and tumor and corresponding fluorescent microscopy of liver and tumor sections. The HCC tumor is highlighted by the dotted circle. Note the intracellular granular punctate fluorescent pattern present in

fluorescent microscopy sections is indicative of the receptor mediated endocytic internalization of the LDL nanoparticles.

Author Manuscript

Author Manuscript

Author Manuscript

Author Manuscript



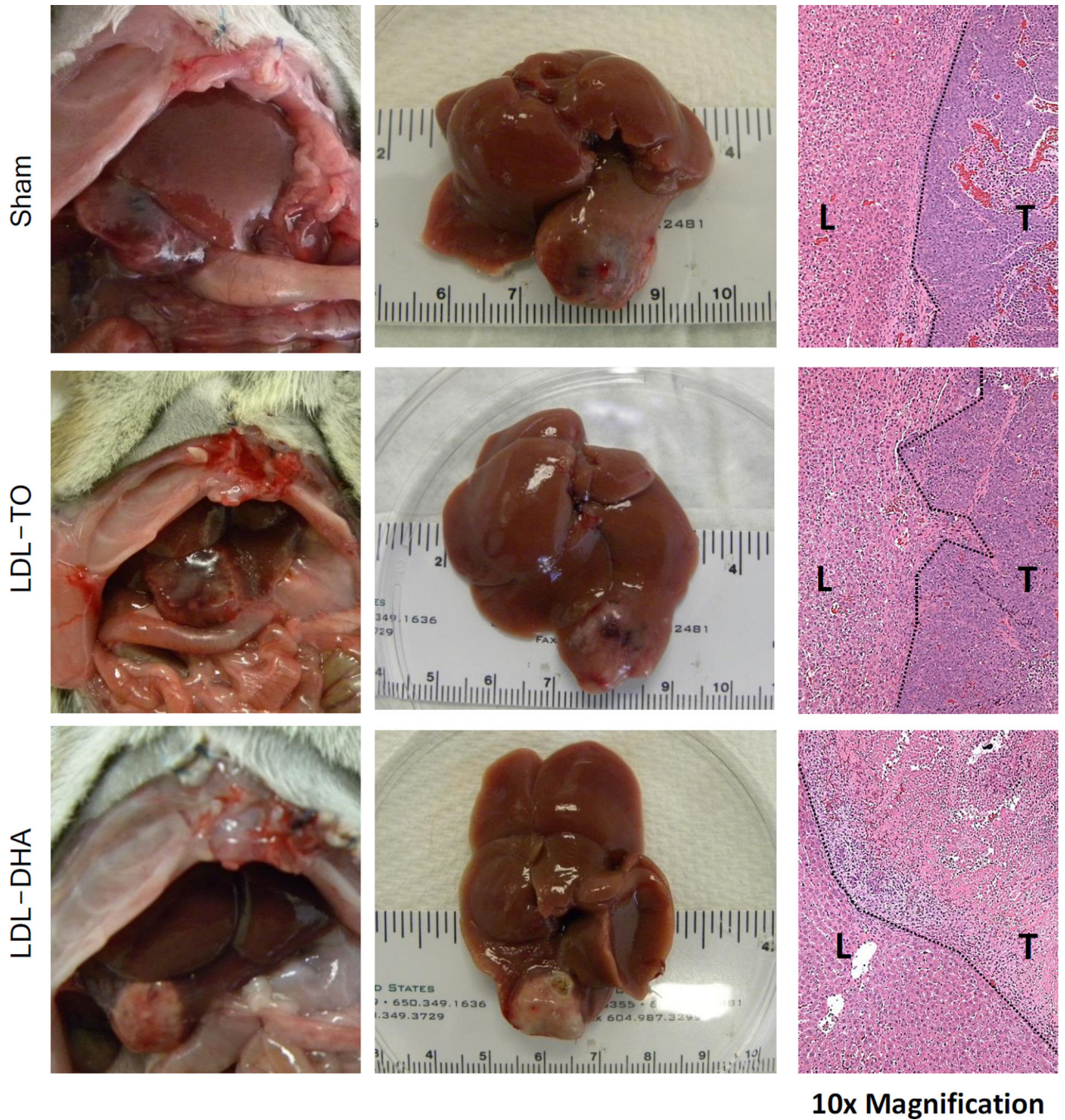


**Figure 3. Therapeutic effect of HAI of LDL-DHA in HCC bearing rats**

In situ (left) and excised (middle) view of liver and H4IIE HCC tumor three days after sham or hepatic artery injection (HAI) with 2 mg/kg of LDL nanoparticles. The right panel shows the corresponding histology at the liver tumor interface (10× magnification). Dotted line indicates liver tumor boundary. HAI, hepatic artery injection.

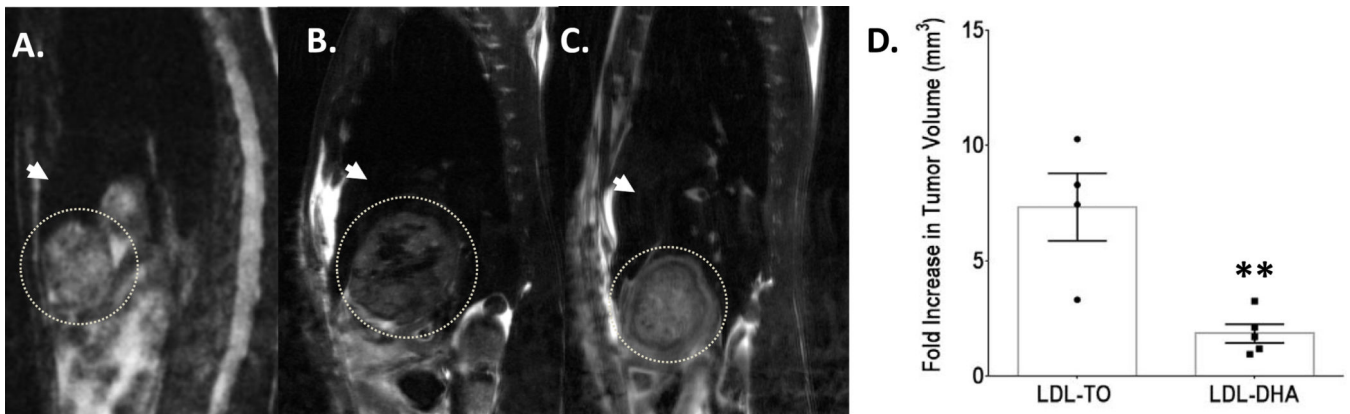


**Figure 4. Assessment of tumors with MRI**

Representative T2-weighted sagittal images of tumor bearing rats (A) before LDL nanoparticle treatment; (B) 72 hours after LDL-TO treatment; and (C) 72 hours after LDL-DHA treatment. The tumor is highlighted by the dotted circle and the white arrow head indicates liver. (D) Changes in tumor volume measured 4–6 days after LDL nanoparticle treatments compared to pre-treatment tumor volume. Data are expressed as mean fold change  $\pm$  SEM. \*\*, P < 0.01 versus LDL-TO treated animals.



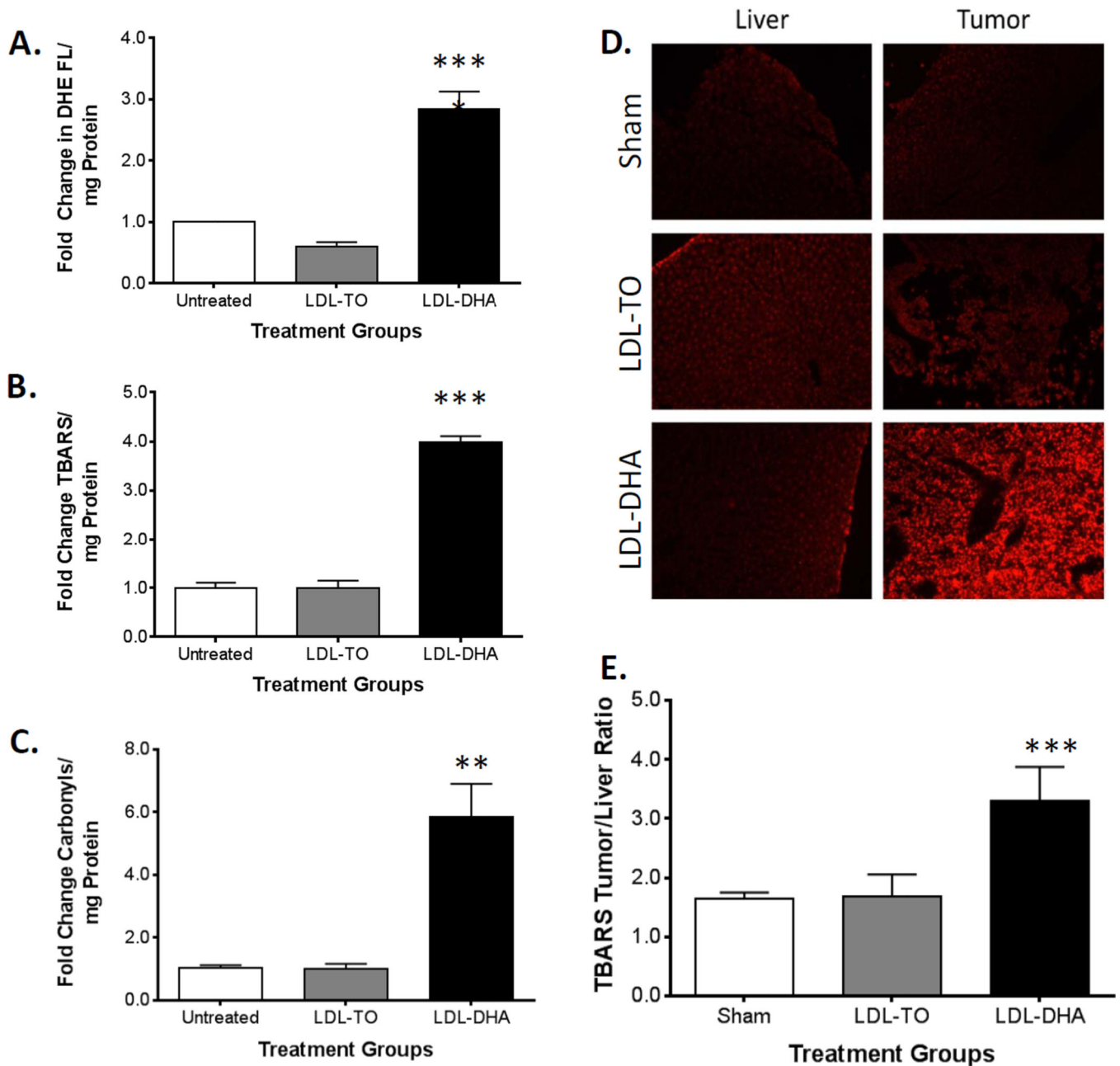


**Figure 5. LDL-DHA increases oxidative stress *in vitro* and *in vivo***

Measures of oxidative stress in H4IIE cell after LDL-DHA treatment. **(A)** Superoxide ROS levels were measured by dihydroethidium fluorescence intensity per mg of cell protein. **(B)** The TBARS assay measured lipid peroxide levels per mg of cell protein. **(C)** Protein carbonyls (mg of cell protein) were detected as 2,4-dinitrophenylhydrazine derivatives. All assays were measured in H4IIE cells at Baseline and 48 hours after 40  $\mu$ M LDL-TO or 40  $\mu$ M LDL-DHA treatment. Data for the assay are normalized to the untreated control to yield fold change and expressed as mean  $\pm$  SEM. *In vivo* superoxide and lipid peroxide levels in HCC 3 days after Sham and HAI treatment of LDL nanoparticles (2 mg/kg). **(D)** Dihydroethidium fluorescence imaging of tissues was performed at 20 $\times$  with Texas Red

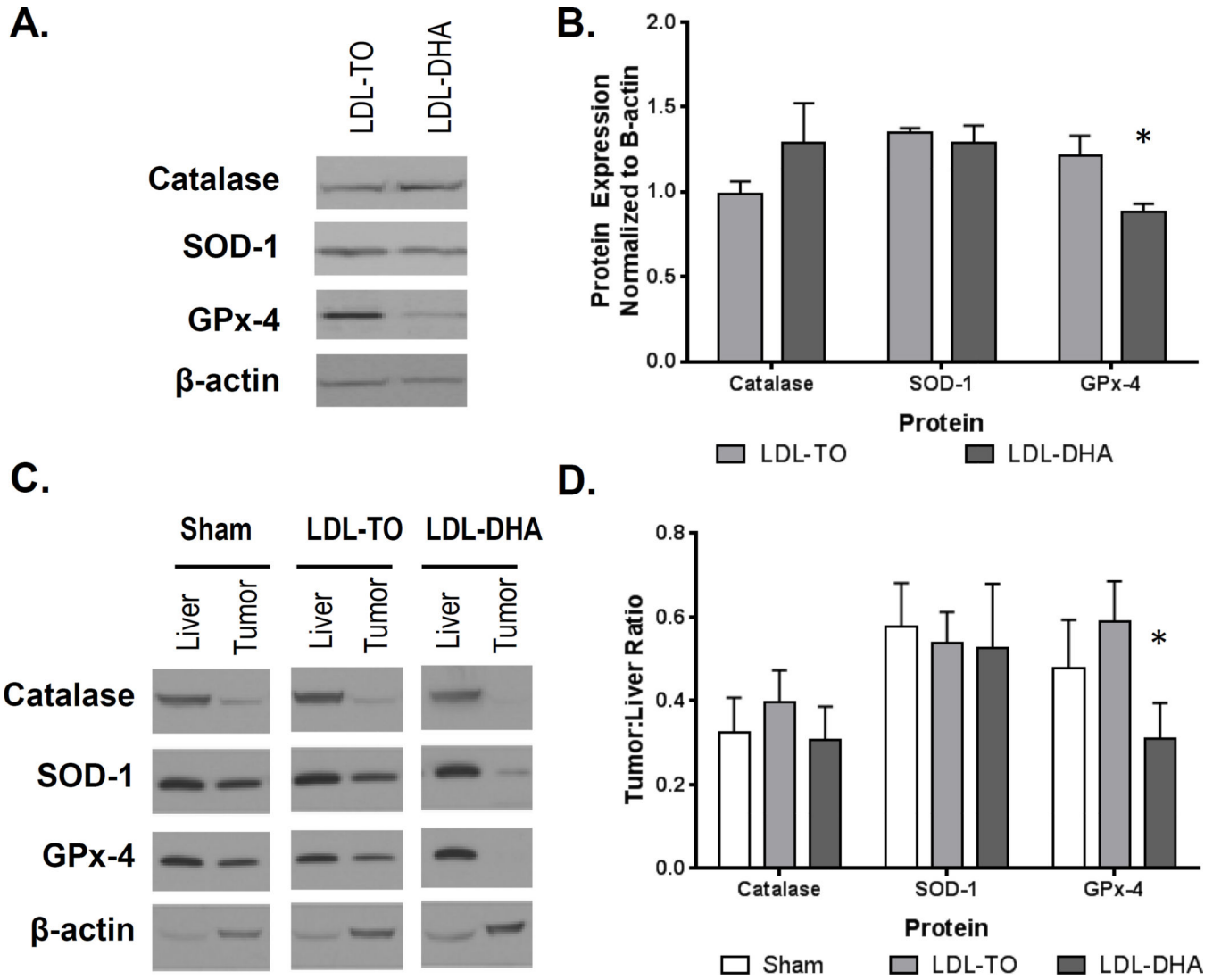
filter ( $\lambda_{ex}=596$ ). **(E)** TBARS reading in liver and H4IIE tumor samples. The data are expressed as a ratio of tumor to liver (mean  $\pm$  SEM) for each treatment group (B). \*, P 0.05; \*\*, P 0.01; \*\*\*, P 0.001; \*\*\*\*, P 0.0001 versus untreated or sham groups.

Author Manuscript

Author Manuscript

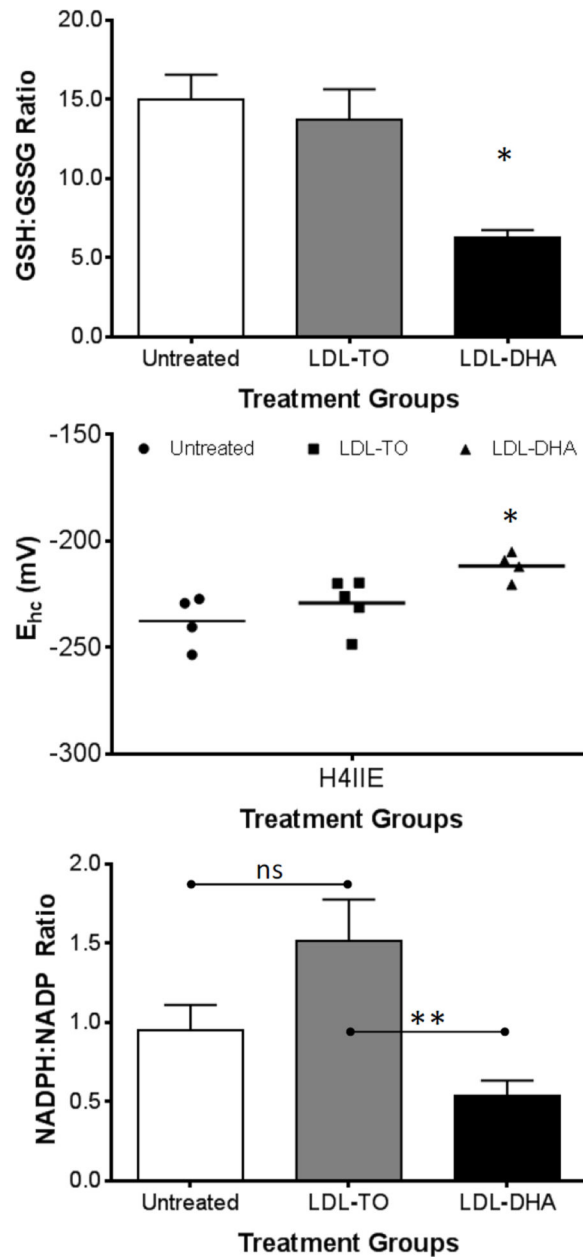
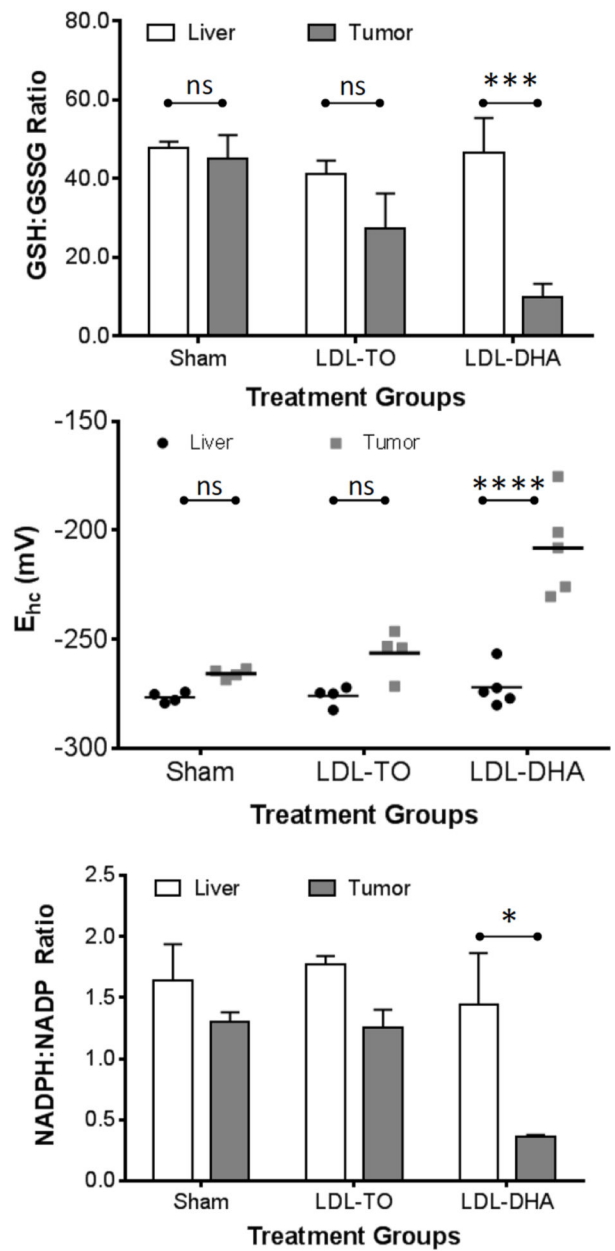
Author Manuscript

Author Manuscript



**Figure 6. *In vitro* and *in vivo* protein expression of catalase, SOD-1 and GPx-4 following LDL nanoparticle treatments**

(A, B) Protein expression levels of enzyme antioxidant 72 hours after LDL nanoparticle (40  $\mu$ M) treatments in H4IIE cells. Representative blots and quantifications are shown. The data are expressed relative to  $\beta$ -actin expression (mean  $\pm$  SEM) for each treatment group. \*, P 0.05 (C,D) Protein expression levels of enzyme antioxidants in rat liver and H4IIE tumor 72 hours after Sham and HAI treatment of LDL nanoparticles (2 mg/kg). Representative blots and quantifications are shown. The data are expressed relative to  $\beta$ -actin expression as a ratio of tumor to liver (mean  $\pm$  SEM) for each treatment group. \*, P 0.05

A. *in vitro*B. *in vivo*

**Figure 7. *In vitro* and *in vivo* redox couples following LDL nanoparticle treatments**  
 (A) GSH/GSSG, glutathione half-cell potential, and NADPH/NADP levels in H4IIE cells at baseline (untreated) and 48 hours after LDL nanoparticle (40  $\mu$ M) treatments. (B) GSH/GSSG, glutathione half-cell potential, and NADPH/NADP levels in rat liver and H4IIE tumor 72 hours after Sham and HAI treatment of LDL nanoparticles (2 mg/kg). The data are expressed as mean  $\pm$  SEM for each treatment group (B). \*,  $P < 0.05$ ; \*\*,  $P < 0.01$ ; \*\*\*,  $P < 0.001$ ; \*\*\*\*,  $P < 0.0001$  versus indicated groups.